J Fluoresc (2011) 21:507–519
DOI 10.1007/s10895-010-0737-7

ORIGINAL PAPER

Iridium(III) Complexes with Orthometalated Phenylimidazole Ligands Subtle Turning of Emission to the Saturated Green Colour

Jayaraman Jayabharathi · Venugopal Thanikachalam · Kanagarathinam Saravanan · Natesan Srinivasan

Received: 27 July 2010 / Accepted: 28 September 2010 / Published online: 16 October 2010

Abstract A series of novel six iridium complexes (**1–6**) bearing two substituted phenylimidazole and an additional acetylacetone as the third co-auxilary ligand are reported. The lowest absorption band for all iridium complexes consist of a mixture of heavy atom Ir(III) enhanced ^{3}MLCT and ^{3} π-π* transitions and the phosphorescent peak wavelength can be fine-tuned to cover the spectral range 455–518 nm with high quantum efficiencies. The peak wavelength of the dopants can be finely tuned depending upon the electronic properties of the substituents. On the basis of onset potentials of the oxidation and reduction, the HOMO-LUMO energies were calculated and the reported iridium complexes emit green light with exceeding higher efficiency.

Keywords MLCT transition · Colour tuning · DFT calculation · HOMO-LUMO orbital · Transphobia

Introduction

Organometallic complexes possessing a third-row transition-metal element are crucial for the fabrication of highly efficient organic light-emitting diodes (OLEDs) [1–3]. The strong spin-orbit coupling induced by a heavy-metal ion such as iridium(III) promotes an efficient intersystem crossing from the singlet to the triplet excited-state manifold which then facilitates strong electroluminescence by the harnessing of both singlet and triplet excitons after the initial charge recombination. Since internal phosphorescence quantum efficiency (h_{int}) of as high as ~100% could theoretically be achieved, these heavy-metal containing emitters would be superior to their fluorescent counterparts in future OLED applications [4–11]. As a result, there is a continuous trend of shifting research endeavors of these heavy transtion metal complexes.

Since the manufacture of a full colour display requires the usage of emitters with all three primary colours, blue, green and red rationally tuning the emission wavelength of heavy-metal phosphorescent emitters over the entire visible range has emerged as an important ongoing research task [12]. Reports on the red-emitting complexes with the Os(II) [13–18] and Pt(II) [19, 20] elements have been documented in the literature. In this paper, we report a systematic design, synthesis and characterization of green-emitting Ir (III) complexes containing substituted phenylimidazole ligands for which, the high rigidity of the ligand framework would significantly reduce the non-radiative transitions.

Experimental

Materials and Methods

Iridium(III) trichloride hydrate ($IrCl_3{\cdot}3H_2O$, Sigma-Aldrich Ltd.), 2-ethoxyethanol ($H_5C_2OC_2H_4OH$, S.D. fine) and all the other reagents used without further purification.

Optical Measurements and Compositions Analysis

The ultraviolet-visible (UV-vis) spectra of the phosphorescent Ir(III) complexes were measured in an UV-vis spectrophotometer (Perkin Elmer Lambda 35) and corrected for background absorption due to solvent. Photoluminescence (PL) spectra were recorded on a (Perkin Elmer LS55) fluorescence

J. Jayabharathi (✉) · V. Thanikachalam · K. Saravanan · N. Srinivasan
Department of Chemistry, Annamalai University, Annamalainagar 608002 Tamilnadu, India
e-mail: jtchalam2005@yahoo.co.in

spectrometer. The solid-state emission spectra were recorded on fluoromax 2 (ISA SPEX) xenon-Arc lamp as a source. NMR spectra were recorded on Bruker 400 MHz NMR spectrometer. MS spectra (EI and FAB) were recorded on a Varian Saturn 2200 GCMS spectrometer. Cyclic voltammetry (CV) analysis were performed by using CHI 630A potentiostap electrochemical analyzer. Measurements of oxidation and reduction were undertaken using 0.1 M tetra(n-butyl)ammonium- hexafluorophosphate as the supporting electrolyte, at scan rate of $0.1 VS^{-1}$. The potentials were measured against an Ag/Ag^+ (0.01 M $AgNO_3$) reference electrode using ferrocene/ferrocenium (CP_2Fe/CP_2Fe^+) as the internal standard. The onset potentials were determined from the intersection of two tangents drawn at the rising current and background current of the cyclic voltammogram.

General Procedure for the Synthesis of Ligands

The various substituted phenylimidazole ligands were prepared from an unusual four components assembling of 1,2-dione, ammonium acetate, arylamine and an arylaldehyde as shown in Scheme 1 [21].

4,5-Dimethyl-1,2-diphenyl-1H-imidazole (dmdpi)

Yield: 48%. ^{1}H NMR (400 MHz, $CDCl_3$): δ 2.07 (s, 3H), 2.35 (s, 3H), 7.22 (m, 5H), 7.37 (m, 2H), 7.48 (m, 3H). ^{13}C NMR (100 MHz, $CDCl_3$): δ 9.50, 12.58, 71.50, 114.2, 117.3, 128.20, 129.58, 144.35. Anal. calcd. for $C_{17}H_{16}N_2$: C, 82.21; H, 6.45; N, 11.28. Found: C, 82.07; H, 6.32; N, 11.04. MS: m/z 248.03, calcd. 248.13.

4,5-Dimethyl-1-(4′-methoxyphenyl)-2-phenyl-1H-imidazole (dmmppi)

Yield: 50%. ^{1}H NMR (400 MHz, $CDCl_3$): δ 2.29 (s, 3H), 2.02 (s, 3H), 3.85 (s, 3H), 6.91–7.10 (aromatic protons). ^{13}C NMR (100 MHz, $CDCl_3$): δ 9.39, 12.59, 55.32, 114.50, 125.51, 127.41, 127.87, 128.78, 130.48, 130.74, 133.12, 145.08, 159.23. Anal. calcd. for $C_{18}H_{18}N_2O$: C, 77.67; H, 6.52; N, 10.06. Found: C, 77.14; H, 6.32; N, 9.87. MS: m/z 278.2, calcd. 278.36.

4,5-Dimethyl-1-(4′-methoxyphenyl)-2-(p-fluorophenyl)-1H-imidazole (dmmpfpi)

Yield: 40%. ^{1}H NMR (400 MHz, $CDCl_3$): δ 2.28 (s, 3H), 1.99 (s, 3H), 3.85 (s, 3H), 6.85–7.35 (aromatic protons). ^{13}C NMR (100 MHz, $CDCl_3$): δ 9.50, 12.69, 55.48, 114.71, 114.93, 115.14, 128.90, 129.80, 130.42, 133.21, 144.36, 159.45. Anal. calcd. for $C_{18}H_{17}N_2OF$: C, 72.95; H, 5.78; N, 9.45. Found: C, 72.24; H, 5.36; N, 8.98. MS: m/z 296.5, calcd. 296.35.

4,5-Dimethyl-1-(3′,5′-dimethoxyphenyl)-2-phenyl-1H-imidazole (dmdmppi)

Yield: 45%. ^{1}H NMR (400 MHz, $CDCl_3$): δ 2.29 (s, 3H), 2.05 (s, 3H), 3.73 (s, 6H), 6.32–7.43 (aromatic protons). ^{13}C NMR (100 MHz, $CDCl_3$): δ 9.36, 12.58, 55.32, 100.21, 106.20, 125.13, 127.45, 127.65, 127.83, 130.68, 133.34, 139.38, 144.79, 161.01. Anal. calcd. for $C_{19}H_{20}N_2O_2$: C, 73.93; H, 6.54; N, 9.08. Found: C, 73.23; H, 6.18; N, 8.79. MS: m/z 308.3, calcd. 308.38.

4,5-Dimethyl-1-(3′,5′-dimethoxyphenyl)-2-(p-fluorophenyl)-1H-imidazole (dmdmpfpi)

Yield: 45%. ^{1}H NMR (400 MHz, $CDCl_3$): δ 2.28 (s, 3H), 2.04 (s, 3H), 3.74 (s, 6H), 6.30–7.40 (aromatic protons). ^{13}C NMR (100 MHz, $CDCl_3$): δ 9.40, 12.58, 55.44, 100.32, 106.25, 114.85, 115.06, 125.23, 127.00, 129.55, 133.38, 139.27, 143.98, 161.18. Anal. calcd. for $C_{19}H_{19}N_2O_2F$: C, 69.92; H, 5.87; N, 8.58. Found: C, 69.12; H, 5.37; N, 8.24. MS: m/z 326.3, calcd. 326.37.

4,5-Dimethyl-1-(4′-t-butylphenyl)-2-(p-fluorophenyl)-1H-imidazole (dmtbpfpi)

Yield: 52%. ^{1}H NMR (400 MHz, $CDCl_3$): δ 1.32 (s, 9H), 1.92 (s, 3H), 2.26 (s, 3H), 6.82 (t, 2H, J=8.4 Hz), 7.04 (d, 2H, J=8 Hz), 7.27 (m, 2H), 7.41 (d, 2H, J=8 Hz). ^{13}C NMR (100 MHz, $CDCl_3$): δ 9.40, 12.58, 31.0, 72.0, 110.30, 125.31, 127.08, 133.89, 142.68. Anal. calcd. for $C_{21}H_{23}N_2F$: C, 78.17; H, 7.13; N, 8.69. Found: C, 78.34; H, 7.03; N, 6.71. MS: m/z 322.2, calcd. 322.39.

General Procedure for the Synthesis of Iridium Complexes (1–6)

The phenylimidazole based cyclometalated iridium complexes **1–6** were readily synthesized from $IrCl_3 \cdot nH_2O$ and the phenylimidazole ligands to give the corresponding dimeric species via the Nonoyama route [22] followed by the treatment with acetylacetone in the presence of K_2CO_3 as shown in Scheme 1.

Iridium(III)bis(4,5-dimethyl-1,2-diphenyl -1H-imidazolato-N,C$^{2\prime}$)(acetylacetonate) ($Ir(dmdpi)_2(acac)$), **1**

Yield: 68%. ^{1}H NMR (400 MHz, $CDCl_3$): δ 7.89 (dd, 2H, J=5.0, 9.0 Hz), 7.71 (dd, 2H, J=5.5, 8.5 Hz), 7.35 (dd, 2H, J=8.5, 11.0 Hz), 7.20 (d, 4 H), 7.06 (t, 2H, J=8.5 Hz), 7.14 (t, 3H, J=8.5 Hz), 6.52 (d, 3H, J=8.5 Hz), 5.31 (s, 1H), 2.24 (s, 3H), 2.06 (s, 3H), 1.36 (s, 6H), 1.20 (s, 6H). ^{13}C NMR (100 MHz, $CDCl_3$): δ 9.41, 10.52, 23.91, 24.48, 25.74, 31.19, 31.31, 34.65, 115.92, 116.13, 116.31, 119.18, 126.12, 126.62, 127.44, 130.06, 130.13, 130.99, 131.06, 136.57, 151.58, 171.66. Anal. calcd. for $C_{39}H_{37}IrN_4O_2$: C,

Scheme 1 Synthesis of ligands and iridium complexes $(C^\wedge N)_2Ir$ (acac) **1–6**

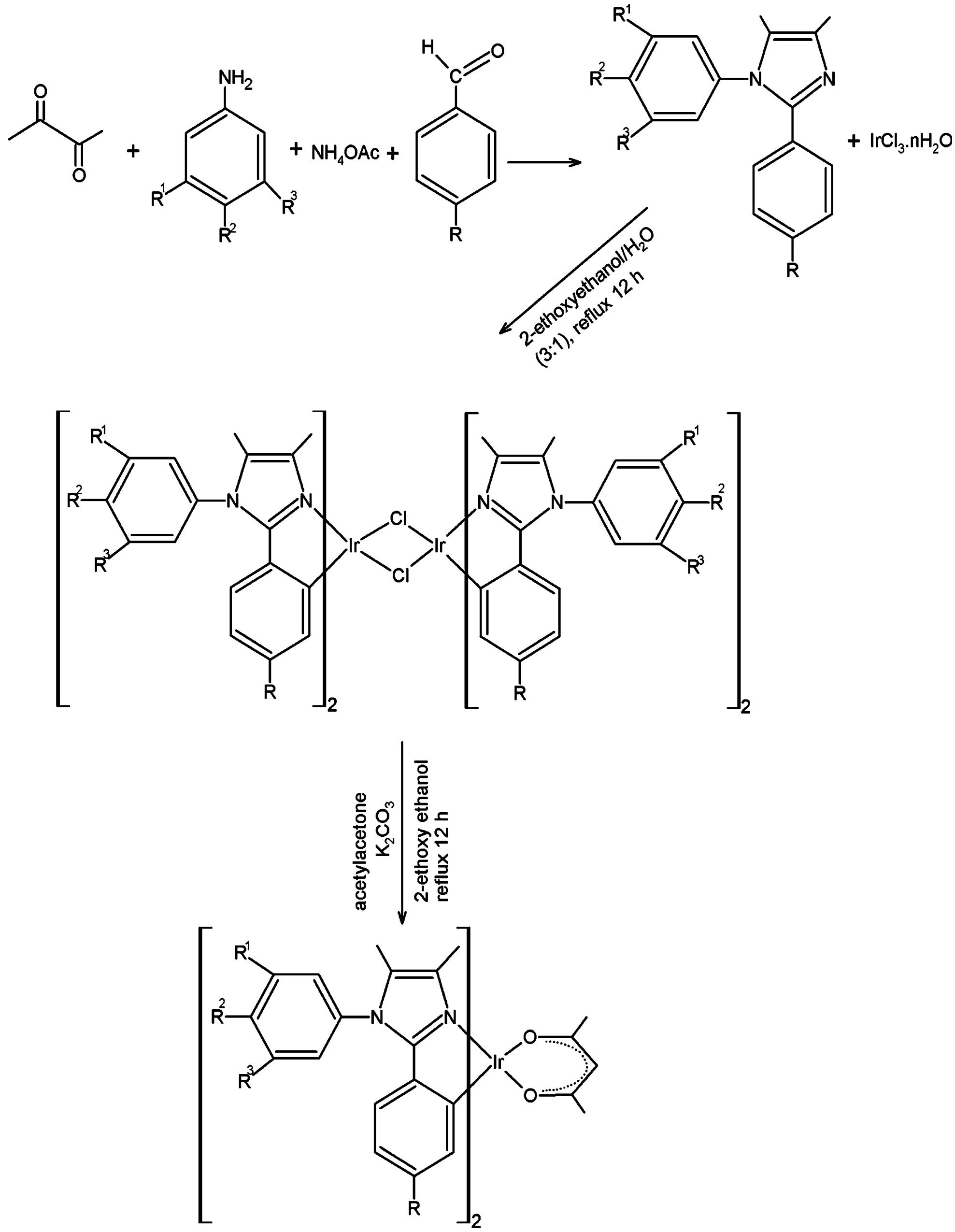

	R	R^1	R^2	R^3
1;	H	H	H	H
2;	H	H	OCH_3	H
3;	F	H	OCH_3	H
4;	H	OCH_3	H	OCH_3
5;	F	OCH_3	H	OCH_3
6;	F	H	t-But	H

59.60; H, 4.75; N, 7.13. Found: C, 59.30; H, 4.35; N, 7.08. MS: m/z 786.05, calcd. 786.25.

Iridium(III)bis(4,5-dimethyl-1-(4′-methoxyphenyl)-2-phenyl-1H-imidazolato-N,$C^{2\prime}$) (acetylacetonate) (Ir $(dmmppi)_2(acac)$), **2**

Yield: 62%. ^1H NMR (400 MHz, $CDCl_3$): δ 7.35 (m, 2H), 7.26 (m, 2H), 7.05 (m, 4H), 6.53 (m, 2H), 6.47 (dd, 2H, J=0.92, 7.53 Hz), 6.38 (m, 2H), 6.15 (dd, 2H, J=0.88, 7.73 Hz), 5.28 (s, 1H), 3.91 (s, 6H), 2.20 (s, 6H), 2.00 (s, 6H), 1.76 (s, 3H), 1.60 (s, 3H), 1.26 (s, 3H). ^{13}C NMR

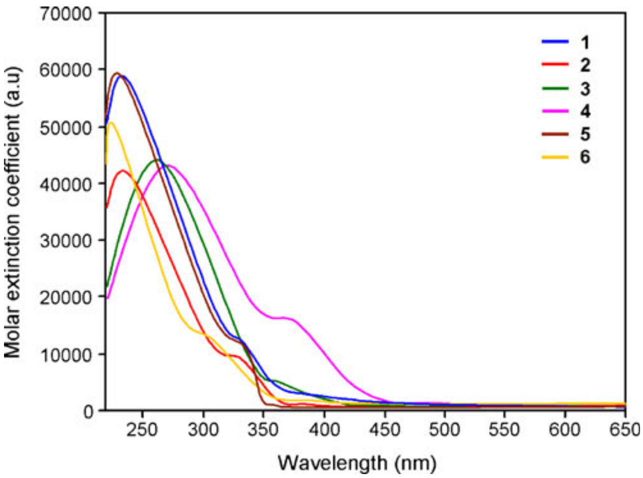

Fig. 1 The UV-vis absorption spectra of the complexes **1–6** in CH_2Cl_2

(100 MHz, $CDCl_3$): δ 9.32, 10.47, 28.32, 29.67, 55.54, 100.67, 114.89, 119.33, 121.57, 123.37, 126.55, 128.23, 128.84, 129.45, 132.38, 134.03, 137.22, 144.86, 157.15, 160.05, 183.92. Anal. calcd. for $C_{41}H_{41}IrN_4O_4$: C, 58.21; H, 4.88; N, 6.62. Found: C, 57.96; H, 4.72; N, 6.48. MS: m/z 846.60, calcd. 846.28.

Iridium(III)bis(4,5-dimethyl-1-(4′-methoxyphenyl)-2-(p-fluorophenyl)-1H-imidazolato-N,C$^{2\prime}$)(acetylacetonate) (Ir(dmmpfpi)$_2$(acac)), **3**

Yield: 75%. ^{1}H NMR (400 MHz, $CDCl_3$): δ 7.32 (d, 1H, J=2.76 Hz), 7.24 (t, 1H, J=2.16 Hz), 7.04 (m, 4H), 6.1 (m, 8H), 5.29 (s, 1H), 3.90 (s, 6H), 2.12 (s, 3H), 2.15 (s, 3H), 1.98 (s, 6H), 1.76 (s, 6H). ^{13}C NMR (100 MHz, $CDCl_3$): δ 9.31, 10.41, 28.26, 55.56, 115.03, 101.04, 106.38, 115.03, 128.91, 129.36, 129.49, 156.30, 160.18, 184.29. Anal. calcd. for $C_{41}H_{39}F_2IrN_4O_4$: C, 55.83; H, 4.46; N, 6.35. Found: C, 55.62; H, 4.35; N, 6.28. MS: m/z 881.40, calcd. 882.26.

Iridium(III)bis(4,5-dimethyl-1-(3′,5′-dimethoxyphenyl)-2-phenyl-1H-imidazolato-N,C$^{2\prime}$)(acetylacetonate) (Ir(dmdmppi)$_2$(acac)), **4**

Yield: 78%. ^{1}H NMR (400 MHz, $CDCl_3$): δ 7.24 (s, 2H), 6.61 (t, 2H, J=2.5 Hz), 6.54 (t, 2H, J=2.5 Hz), 6.45 (t, 2H, J=2.5 Hz), 6.24 (dd, 2H, J=7.5, 11.0 Hz), 6.13 (d, 2H, J=2.5 Hz,), 6.07 (dd, 2H, J=3.5, 13.0 Hz), 5.29 (s, 1H), 3.80 (s, 6H), 3.77 (s, 6H), 2.16 (s, 6H), 2.03 (s, 6H), 1.77 (s, 3H), 1.56 (s, 3H). ^{13}C NMR (100 MHz, $CDCl_3$): δ 9.63, 14.09, 22.68, 29.69, 55.74, 101.84, 106.30, 119.56, 126.0, 132.08, 134.11, 138.76, 161.89, 163.86, 187.02. Anal. calcd. for $C_{43}H_{45}IrN_4O_6$: C, 57.00; H, 5.01; N, 6.18. Found: C, 56.82; H, 4.98; N, 6.02. MS: m/z 905.82, calcd. 906.30.

Iridium(III)bis(4,5-dimethyl-1-(3′,5′-dimethoxyphenyl)-2-(p-fluorophenyl)-1H-imidazolato-N,C$^{2\prime}$)(acetylacetonate) (Ir(dmdmpfpi)$_2$(acac)), **5**

Yield: 72%. ^{1}H NMR (400 MHz, $CDCl_3$): δ 6.63 (t, 2H, J=2.26 Hz), 6.57 (t, 2H, J=1.97 Hz), 6.47 (t, 2H, J=1.93 Hz), 6.62 (dd, 2H, J=5.88, 8.52 Hz), 6.15 (m, 2H), 6.10 (dd, 2H, J=2.56, 10.41 Hz), 5.31 (s, 1H), 3.82 (s, 6H), 3.79 (s, 6H), 2.18 (s, 6H), 2.05 (s, 6H), 1.79 (s, 3H), 1.26

Table 1 Photophysical properties of iridium complexes **1–6**

Complex	Absorption[a] (λ, nm) (log ε)	Emission[b] (λ, nm)	Quantum yield (φ)	Lifetime (μs)	k_r	k_{nr}
Ir(dmdpi)$_2$(acac), **1**	230.0 (4.77) 331.0 (4.07) 393.0 (3.23)	455	0.08	2.3	0.03	0.40
Ir(dmmppi)$_2$(acac), **2**	231.0 (4.63) 328.0 (3.93) 389.0 (3.26)	502	0.28	2.4	0.12	0.30
Ir(dmmpfpi)$_2$(acac), **3**	260.0 (4.60) 356.0 (3.62) 450.0 (2.83)	508	0.34	2.3	0.15	0.28
Ir(dmdmppi)$_2$(acac), **4**	269.0 (4.65) 369.0 (4.22) 489.0 (3.34)	510	0.43	1.8	0.24	0.32
Ir(dmdmpfpi)$_2$(acac), **5**	228.0 (4.79) 335.0 (4.07) 356.0 (3.23)	518	0.49	1.5	0.33	0.34
Ir(dmtbpfpi)$_2$(acac), **6**	222.0 (4.72) 301.0 (4.12) 392.0 (3.20)	498	0.25	2.2	0.11	0.34

[a] UV-vis absorption measured in CH_2Cl_2 solution, concentration=1×10^{-5} M.

[b] Photoluminescence measured in CH_2Cl_2 solution, concentration=1×10^{-4} M.

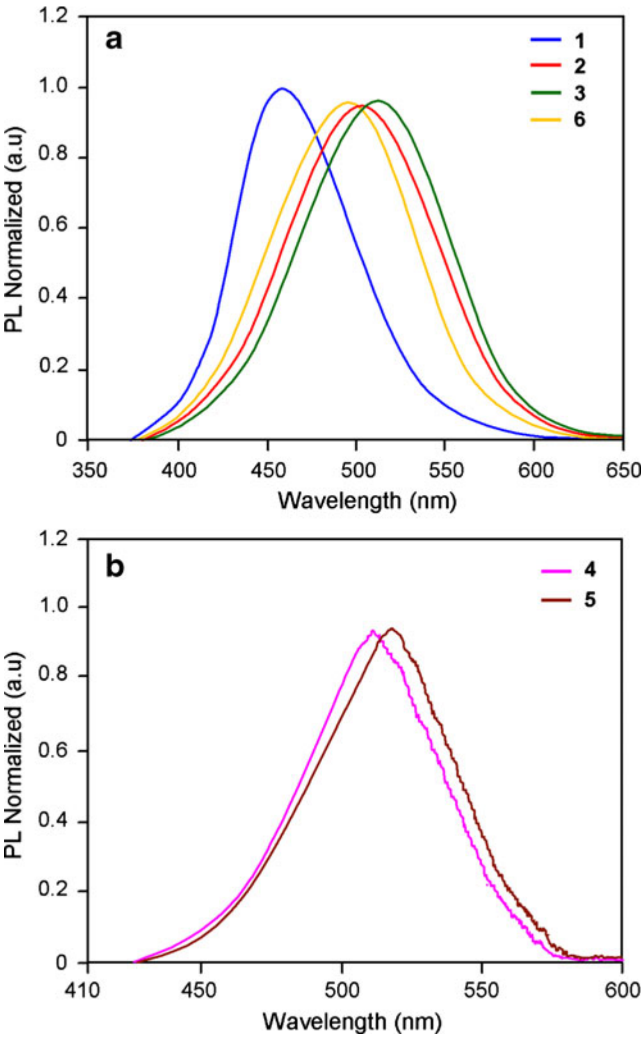

Fig. 2 **a** The photoluminescence emission spectra of the complexes **1**, **2**, **3** and **6** in CH_2Cl_2 and **b** the photoluminescence emission spectra of the complexes **4** and **5** in CH_2Cl_2

(s, 3H). [13]C NMR (100 MHz, $CDCl_3$): δ 9.25, 10.26, 29.69, 55.72, 100.97, 102.06, 106.22, 106.47, 119.95, 120.11, 123.01, 123.31, 132.26, 133.16, 137.94, 161.63, 184.27. Anal. calcd. for $C_{43}H_{43}F_2IrN_4O_6$: C, 54.82; H, 4.60; N, 5.95. Found: C, 54.63; H, 4.38; N, 5.78. MS: m/z 941.98, calcd. 942.04.

Iridium(III)bis(4,5-dimethyl-1-(4′-t-butylphenyl)-2-(p-fluorophenyl)-1H-imidazolato-N,$C^{2\prime}$)(acetylacetonate) (Ir(dmtbpfpi)$_2$(acac)), **6**

Yield: 72%. [1]H NMR (400 MHz, $CDCl_3$): δ 7.56 (m, 2H), 7.55 (d, 2H, *J*=4.5 Hz), 7.26 (m, 2H), 6.07 (m, 8H), 5.31 (s, 1H), 2.19 (s, 6H), 2.00 (s, 6H), 1.99 (s, 3H), 1.60 (s, 3H), 1.42 (s, 18H). [13]C NMR (100 MHz, $CDCl_3$): δ 9.51, 12.92, 29.30, 32.52, 72.89, 100.68, 112.82, 125.8, 131.12, 138.81, 160.92, 187.32. Anal. calcd. for $C_{47}H_{51}F_2IrN_4O_2$: C, 60.43; H, 5.50; N, 6.00. Found: C, 60.16; H, 5.28; N, 5.83. MS: m/z 934.12, calcd. 934.36.

Theoretical Calculations

All calculations were performed using density functional theory (DFT) as implemented in the Gaussian 03 program [23]. The geometry optimization was carried out by B3LYP level using LANL2Z basis set [24].

Results and Discussion

Absorption Spectra

Figure 1 shows the absorption spectra of iridium complexes **1–6**, the intense band observed in the ultraviolet region (220–270 nm) can be assigned to the allowed ligand-centered (LC) (π-π*) transition [25] of the phenylimidazole ligand since free ligands show absorption around similar wavelength region. Somewhat weaker bands are observed in the lower part of energy around 300–490 nm are not observed in the spectra of free ligands. The band position, size and extinction coefficients suggest that these are metal-to-ligand charge transfer (MLCT) transitions [10, 25–30] and the same assignment is likely here [25–28]. Therefore metal-to-ligand charge transfer transitions ^{1}MLCT and ^{3}MLCT have been resolved in the range of 300–490 nm as indicated in Table 1. Absorption in the range around 300–369 nm for all the complexes correspond to the transition of the ^{1}MLCT state as evident from its extinction coefficient of the order 10^3. The long tail toward lower energy around 380–489 nm are assigned to ^{3}MLCT transitions and gains intensity by mixing with the higher lying ^{1}MLCT transitions through the spin-orbit coupling of Iridium(III) [27, 28].

Photoluminescence Properties

The emission spectra in CH_2Cl_2 at ambient temperature for all six iridium complexes **1–6** are shown in Figs. 2a, b and Table 1 summarizes the luminescent data of complexes **1–6**. In solution, complexes **1–6** have emission maxima around 455, 502, 508, 510, 518 and 498 nm, respectively. Introduction of substituent [31] in the *para* and *meta* positions of the phenyl ring attached to the nitrogen of the imidazole ring produces the red shift in the emission spectra by 43–63 nm. In the case of *p*-methoxy substituted iridium complexes [Ir(dmmppi)$_2$(acac) (**2**) and Ir(dmmpfpi)$_2$(acac) (**3**)] red shift was observed when compared with unsubstituted iridium complex Ir(dmdpi)$_2$(acac) (**1**) by means of 47 and 53 nm, respectively. This may be due to the mesomeric effect exerted by the *p*-methoxy substituent so that resonance interaction between the imidazole ring and the methoxy substituted aryl ring increased and this causes the red shift in the emission spectra (Figs. 2a and b). When

Table 2 Photoluminescence spectral data of various solvents and solid emission spectra of complexes **1–6**

Solvent	Absorption[a] (λ, nm) (log ε)						Emission[b] (λ, nm)					
	1	**2**	**3**	**4**	**5**	**6**	**1**	**2**	**3**	**4**	**5**	**6**
n-Hexane	228.0 (4.66) 330.0 (3.92) 390.0 (3.19)	229.0 (4.52) 326.0 (3.93) 287.0 (3.19)	258.0 (4.61) 353.0 (3.59) 459.0 (2.77)	267.0 (4.61) 368.0 (4.17) 487.0 (3.30)	229.0 (4.72) 334.0 (3.99) 357.0 (3.11)	220.0 (4.65) 299.5 (3.98) 391.0 (3.14)	436	481	480	485	487	482
Benzene	228.0 (4.62) 330.0 (3.96) 391.0 (3.20)	228.0 (4.59) 325.0 (3.91) 388.0 (3.28)	259.5 (4.53) 354.0 (3.66) 450.0 (2.79)	269.0 (4.67) 369.0 (3.59) 487.0 (3.32)	228.0 (4.76) 335.0 (3.98) 356.0 (3.15)	222.0 (4.30) 299.0 (4.01) 391.5 (3.08)	443	486	489	491	490	486
Chloroform	229.0 (4.62) 331.0 (3.94) 390.0 (3.17)	228.5 (4.57) 326.5 (3.87) 388.0 (3.23)	259.0 (4.56) 355.0 (3.61) 450.5 (2.76)	267.0 (4.71) 368.0 (4.23) 490.0 (3.35)	229.0 (4.81) 334.0 (4.13) 357.5 (3.14)	221.5 (4.69) 298.0 (3.99) 391.0 (3.19)	449	490	496	498	498	492
Ethyl acetate	229.0 (4.71) 331.0 (4.01) 392.0 (3.19)	230.0 (4.60) 327.0 (3.90) 389.0 (3.29)	260.0 (4.69) 356.0 (3.73) 450.0 (2.80)	268.0 (4.61) 367.0 (4.28) 489.0 (3.39)	230.0 (4.78) 335.5 (4.09) 356.0 (3.19)	222.0 (4.79) 300.0 (4.07) 392.0 (3.12)	451	497	503	506	512	494
Dichloromethane	230.0 (4.77) 331.0 (4.07) 393.0 (3.23)	231.0 (4.63) 328.0 (3.93) 389.0 (3.26)	260.0 (4.60) 356.0 (3.62) 450.0 (2.83)	269.0 (4.65) 369.0 (4.22) 489.0 (3.34)	228.0 (4.79) 335.0 (4.07) 356.0 (3.23)	222.0 (4.72) 301.0 (4.12) 392.0 (3.20)	455	502	508	510	518	498
1-Butanol	230.5 (4.79) 330.0 (3.98) 392.0 (3.27)	231.0 (4.61) 328.0 (3.95) 390.0 (3.28)	261.0 (4.68) 356.0 (3.64) 451.0 (2.81)	270.0 (4.70) 369.5 (4.20) 491.0 (3.34)	230.0 (4.80) 337.0 (4.06) 356.5 (3.29)	223.0 (4.81) 301.0 (4.16) 391.0 (3.23)	456	504	509	512	520	499
1-Propanol	230.0 (4.69) 332.0 (4.06) 393.0 (3.20)	230.0 (4.60) 329.0 (3.87) 392.0 (3.32)	260.5 (4.59) 356.0 (3.60) 449.0 (2.78)	271.0 (4.69) 370.0 (4.19) 490.0 (3.31)	229.0 (4.83) 336.5 (4.14) 358.0 (3.30)	222.0 (4.76) 302.0 (4.19) 391.5 (3.19)	458	507	511	515	522	501
Ethanol	231.0 (4.73) 330.0 (3.98) 391.0 (3.24)	231.5 (4.64) 329.0 (3.94) 391.0 (3.16)	260.5 (4.63) 356.0 (3.70) 450.0 (2.89)	270.0 (4.73) 368.0 (3.70) 489.5 (3.39)	329.5 (4.84) 335.0 (4.03) 357.0 (3.24)	221.5 (4.79) 301.0 (4.20) 393.0 (3.31)	459	510	514	518	524	505
Acetonitrile	231.0 (4.82) 332.0 (4.07) 391.0 (3.23)	232.0 (4.65) 328.0 (3.95) 390.0 (3.30)	261.0 (4.70) 358.0 (3.68) 450.5 (2.84)	268.5 (4.71) 370.0 (4.25) 4.90 (3.37)	230.0 (4.86) 336.0 (4.12) 357.0 (3.27)	222.0 (4.75) 301.5 (4.11) 393.0 (3.28)	461	511	515	519	527	506
Solid emission spectra							436.5	481	479	484	488	482

[a] UV-vis absorption measured in solution concentration=1×10^{-5} M.

[b] Photoluminescence measured in solution concentration=1×10^{-4} M.

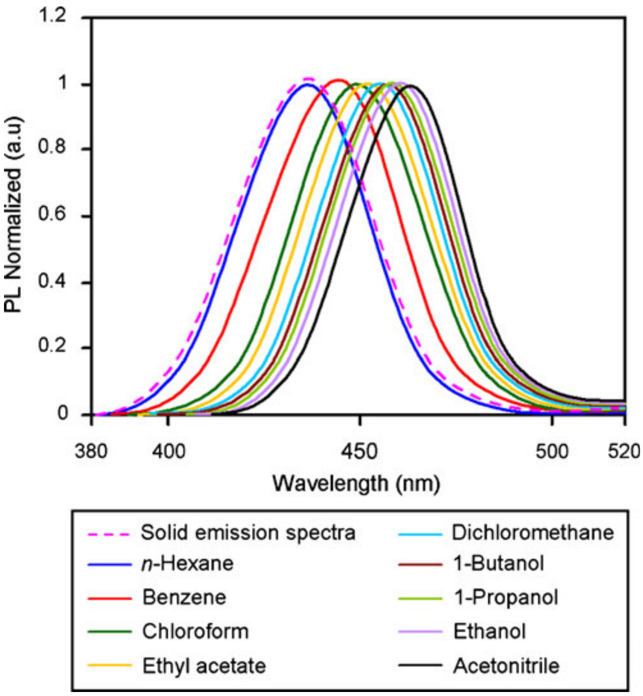

Fig. 3 The solid state and the solvatochromic emission spectra of the complex **1**

on dimethoxy group introduced [Ir(dmdmppi)$_2$(acac) (**4**) and Ir(dmdmpfpi)$_2$(acac) (**5**)] the emission is still maximum due to the additional electronic effect imparted by the methoxy substitutents at 3′ and 5′.

Solvatochromism of the Complexes 1–6

The absorption peak of the complexes **1–6** are almost same in different solvents. This suggests that the polarity of the solvent has very little influence on the ground state energy level of the complexes (Table 2). However variation in the emission peak of the complexes **1–6** was observed in different solvents. The representative spectra of complex **1** are shown in Fig. 3. The emission peak of the complexes **1–6** are 436–487 nm in hexane, 459–524 nm in ethanol, 455–518 nm in CH_2Cl_2 and 461–527 nm in CH_3CN. The peak shift may be due to the stronger interaction between the solvents and the excited state molecules. The excited state of all iridium complexes are more stabilized in polar solvents than in non-polar solvents which leads to red shift of emission with increasing solvent polarity [32]. The photoluminescent peak of solid state (representative spectrum of complex **1** is shown in Fig. 3) of all complexes are almost similar to that of emission in non-polar solvent (*n*-hexane) which shows that there is very little or no influence of molecular interaction on the excited state of iridium complexes in the solid state [32].

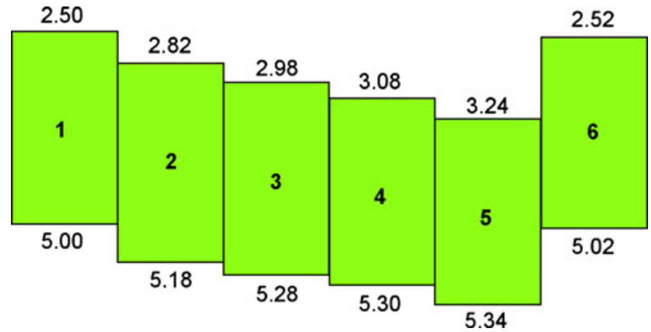

Fig. 4 HOMO-LUMO energy levels of the complexes **1–6**

HOMO-LUMO Energies

The electrochemical properties of the cyclometalated iridium complexes were examined by cyclic voltammetry. The redox potentials were measured relative to an internal ferrocene reference (Cp_2Fe/Cp_2Fe^+=0.45 V *versus* SCE in CH_2Cl_2 solvent) [33, 34] are given in Table 3. As revealed previously [35, 36] the reductions occur primarily on the more electron accepting heterocyclic portion of the cyclometalated C^N ligands whereas the oxidation process is generally considered to largely involve the Ir-phenyl centre. The energies of the highest occupied molecular orbital (HOMO) and lowest unoccupied molecular orbital (LUMO) were calculated using the following Eqs. 1 and 2 [33, 34] and the calculated values are given in Table 3.

$$E_{\mathrm{HOMO}} = 4.4 + E_{(onset)} \tag{1}$$

$$E_{\mathrm{LUMO}} = E_{\mathrm{HOMO}} - 1239/\lambda_{\mathrm{abs}} \tag{2}$$

The iridium complexes show reversible oxidation behaviour and these complexes exhibit HOMO levels ranging of

Table 3 Cyclic voltammetry data of the complexes **1−6**

Complex	$E_{(onset)}$ (V)	HOMO (eV)	LUMO[a] (eV)	E_g (eV)
Ir(dmdpi)$_2$(acac), **1**	0.20	−5.00	−2.50	2.50
Ir(dmmppi)$_2$(acac), **2**	0.38	−5.18	−2.82	2.36
Ir(dmmpfpi)$_2$(acac), **3**	0.48	−5.28	−2.98	2.30
Ir(dmdmppi)$_2$(acac), **4**	0.50	−5.30	−3.08	2.22
Ir(dmdmpfpi)$_2$(acac), **5**	0.54	−5.34	−3.24	2.10
Ir(dmtbpfpi)$_2$(acac), **6**	0.22	−5.02	−2.52	2.50

[a] Measurement was carried out in CH_2Cl_2 solution, concentration= 1×10^{-3} M.

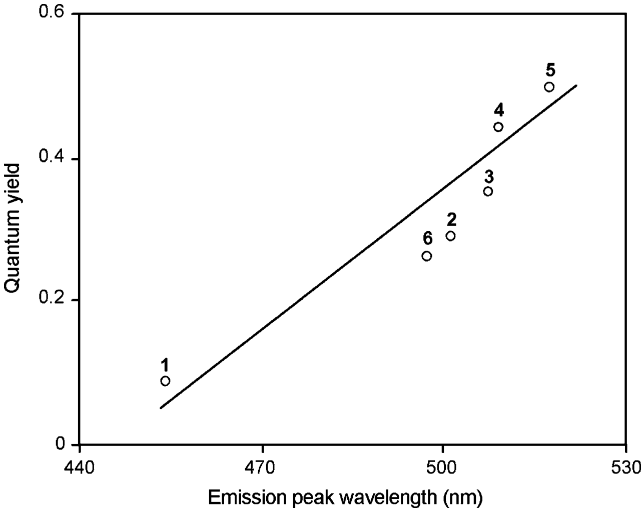

Fig. 5 The plot of quantum yield *versus* emission peak wavelength of the complexes **1–6**

5.00–5.34 eV. The HOMO level of complexes **3–5** are higher than those reported for other iridium complexes [5.2 eV for $Ir(ppy)_2(acac)$ and 5.16 eV for $Ir(btp)_2(acac)$] [12, 25, 36, 37]. The LUMO energies were calculated based on the HOMO energies and the lowest-energy absorption edges of the UV-vis absorption spectra [34]. The calculated energy gap (E_g=HOMO-LUMO) (Fig. 4) for complexes **2–5** are minimum whereas complexes [$Ir(dmdpi)_2(acac)$ (**1**) and $Ir(dmtbpfpi)_2(acac)$ (**6**)] exhibit maximum energy gap. These results reveal that the methoxy substituted complexes **2–5** show emission with the maximum wavelength [502 (**2**), 508 (**3**), 510 (**4**) and 518 nm (**5**)] (minimum E_g) whereas complexes [$Ir(dmdpi)_2(acac)$ (**1**) and $Ir(dmtbpfpi)_2(acac)$ (**6**)] (maximum E_g) exhibit emission with shorter wavelength [455 (**1**) and 498 nm (**6**)].

Effect of Substituent in the Phenyl Ring on HOMO

In the present study iridium complexes **2–6** have electron releasing substituents on the phenyl ring attached to the nitrogen atom of the phenylimidazole ligand and electron withdrawing substituent (i.e., fluorine) on the phenyl ring attached to the carbon atom of the imidazole ligand. It is obvious that the HOMO level of complexes **1–6** is strongly affected by a kind and number of substituent on the phenyl ring attached to the carbon atom of the imidazole moiety (Table 3). Comparison of HOMO values of the iridium complexes reveals that the HOMO values are higher for **2**, **3**, **4** and **5** than complexes **1** and **6**. This may be due to the inductive effect exerted by substituent causes stabilization of iridium complexes through the carbon atom-iridium bonding. Therefore the HOMO stability and the emission energy gap are controlled by the nature of substituents and its inductive influence on the aromatic ring [38].

Quantum Yield and Photochemical Properties

All these complexes **2–6** having larger quantum yield ranging from 0.25–0.49 than unsubstituted iridium complex $Ir(dmdpi)_2(acac)$ (0.08) (**1**) (Table 1). The quantum yield has a tendency to shift to higher with increasing the maximum emission peak wavelength (Fig. 5). The PL quantum yield for all iridium complexes **1–6** were measured in dichloromethane using coumarin 47 in ethanol as a standard [39] according to the Eq. 3,

$$\phi_{\text{unk}} = \phi_{\text{std}}\left(\frac{I_{\text{unk}}}{I_{\text{std}}}\right)\left(\frac{A_{\text{std}}}{A_{\text{unk}}}\right)\left(\frac{\eta_{\text{unk}}}{\eta_{\text{std}}}\right)^2 \quad (3)$$

Where ϕ_{unk} is the fluorescence quantum yield of the sample, ϕ_{std} is the fluorescence quantum yield of the standard, I_{unk} and I_{std} are the integrated emission intensities of the sample and the standard, respectively. A_{unk}, *and* A_{std} are the absorbances of the sample and the standard at the excitation wavelength, respectively. η_{unk} and η_{std} are the indexes of refraction of the sample and standard solutions. The quantum yield for complexes **3**, **4** and **5** are close to the value of 0.40 for $Ir(ppy)_3$ and the photoluminescent lifetime for all iridium complexes **1–6** are reported in Table 1 (Fig. 6). Since these values are comparable to that of $Ir(ppy)_3$ (0.40) [40, 41] which strongly support that these iridium complexes **1–6** are highly phosphorescent emitters.

The radiative and non-radiative rate constants k_r and k_{nr} are calculated from the phosphorescence yield (Φ_p) and the phosphorescence lifetime (τ) using the following Eq. 4,

$$\Phi_p = \Phi_{isc}\{k_r/(k_r + k_{nr})\} \quad (4)$$

Where, Φ_{isc} is the intersystem crossing yield. For iridium complexes Φ_{isc} is safely assumed to be 1.0 because of the strong spin-orbit interaction caused by heavy atom effect of iridium [27, 28]. Thus,

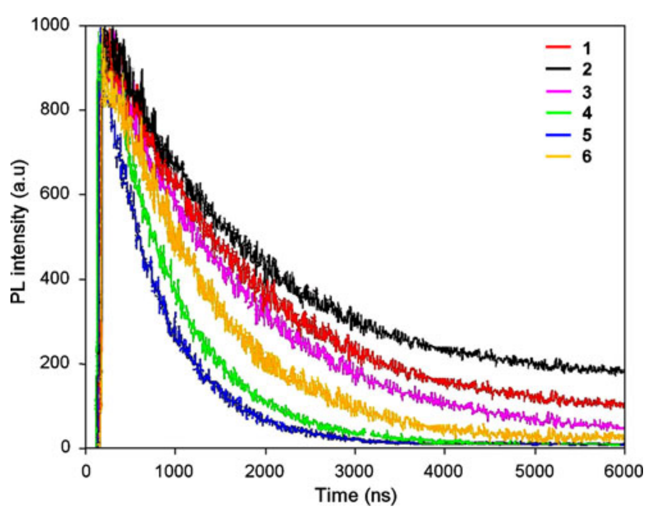

Fig. 6 The lifetime spectra of the complexes **1–6** in CH_2Cl_2

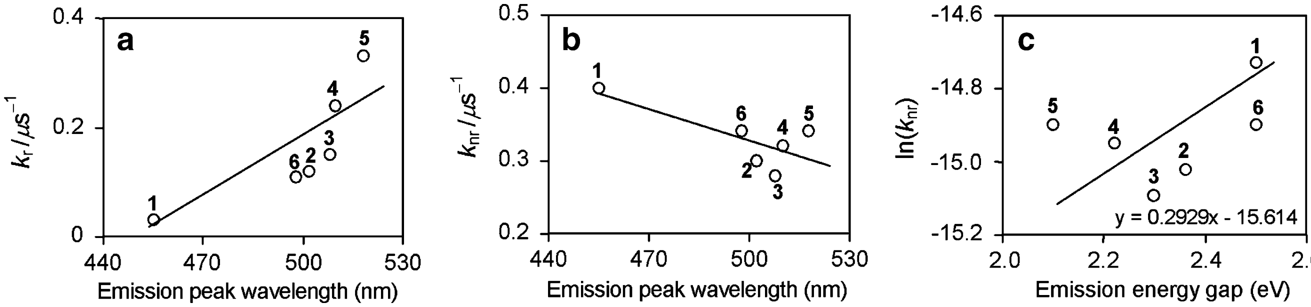

Fig. 7 Quantum yield and decay rate constant of the complexes. **a** Radiative decay rate constant *versus* emission peak wavelength, **b** non-radiative decay rate constant *versus* emission peak wavelength and **c** the plot of $\ln(k_{nr})$ *versus* emission energy gap

$$k_r = \Phi_p / \tau \tag{5}$$

$$k_{nr} = 1/\tau - \Phi_p/\tau \tag{6}$$

$$\tau = (k_r + k_{nr})^{-1} \tag{7}$$

From the viewpoint of the relationship between maximum emission peak wavelength of photoluminescent spectra and decay rate constants, two trends are evident for the iridium complexes **1–6**. The radiative rate constant (k_r) increases with increase in the red shift however the non-radiative decay rate constant (k_{nr}) dose not show monotonous change i.e., nearly same for all complexes [38] (Figs. 7a and b).

The plot of $\ln(k_{nr})$ *versus* the energy gap for complexes **1–6** (Fig. 7c) shows no linear relationship and there is no agreement with the "Energy gap Law". The energy gap law predicts that the rate of non radiative decay increases when the energy gap decreases. This relation is based on the vibrational overlap between the ground state and the excited state and k_{nr} is a function of a Franck-Condon overlap integral [38, 39, 42, 43].

Lastly the radiative decay rate constant of complexes Ir(dmdmppi)$_2$(acac) (**4**) and Ir(dmdmpfpi)$_2$(acac) (**5**) are higher than those of complexes **1–3** and **6**. This may be due to the changes of the mixing states. Consequently complexes Ir(dmdmppi)$_2$(acac) (**4**) and Ir(dmdmpfpi)$_2$(a-cac) (**5**) have large quantum yield rather than complexes **1–3** and **6**. Thompson et al. [19] have concluded that shorter lifetime and stronger *trans* effect would cause lower

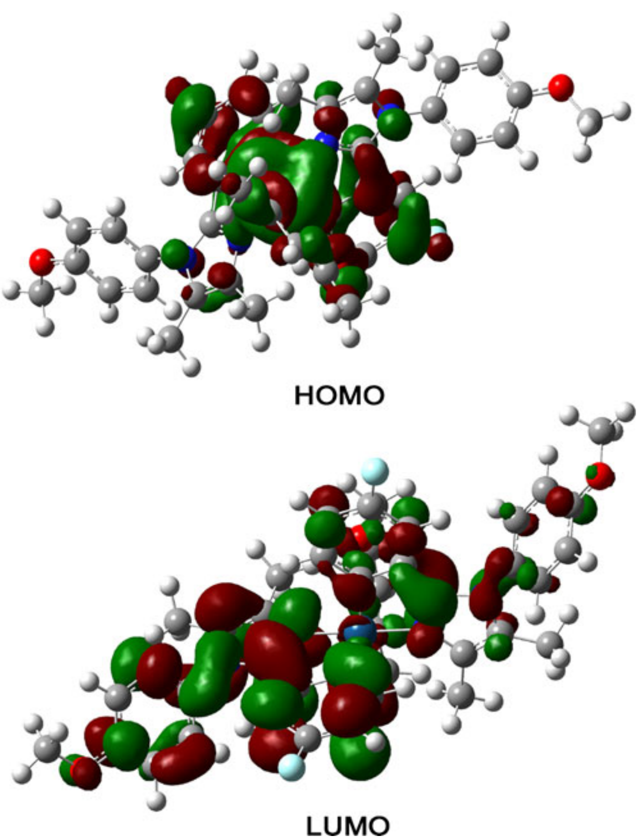

Fig. 8 The HOMO-LUMO orbital picture for the complex Ir (dmmpfpi)$_2$(acac) (**3**)

Fig. 9 Solution colour of the photoluminescence for complexes **4** and **5**

Table 4 Selected bond distance (Å) and bond angles (°) of iridium complexes **3** and **5**

Complex	Atom(1)−Atom(2)	Distance (Å)	Atom(1)−Atom(2)−Atom(3)	Bond angles (°)
$Ir(dmmpfpi)_2(acac)$, **3**	Ir(1)–C(10)	2.0197	Ir(1)–N(4)–C(16)	113.99
	Ir(1)–C(4)	2.0513	Ir(1)–C(8)–C(33)	116.54
	Ir(1)–N(28)	2.0161	Ir(1)–N(6)–C(28)	49.81
	Ir(1)–N(2)	2.0472	Ir(1)–N(4)–C(10)	49.57
	Ir(1)–O(9)	2.1695		
	Ir(1)–O(8)	2.1265		
$Ir(dmdmpfpi)_2(acac)$, **5**	Ir(1)–C(8)	2.0197	N(4)–Ir(1)–C(8)	94.04
	Ir(1)–C(25)	2.0160	N(4)–Ir(1)–C(25)	79.19
	Ir(1)–N(2)	2.0512	Ir(1)–N(4)–C(31)	115.00
	Ir(1)–N(4)	2.0471	Ir(1)–N(2)–C(14)	113.99
	Ir(1)–O(6)	2.1695		
	Ir(1)–O(7)	2.1264		

quantum efficiency in the iridium complexes and similar trend is observed in the case of *para* substituted iridium complexes $Ir(dmmppi)_2(acac)$ (**2**) and $Ir(dmtbpfpi)_2(acac)$ (**6**). The $Ir(dmmppi)_2(acac)$ (**2**) complex have longer emission decay lifetime and consequently much larger luminescence efficiency than the $Ir(dmtbpfpi)_2(acac)$ (**6**) complex having shorter lifetime and longer quantum efficiency.

The Mixing of Excited States

The photophysical properties of complexes **1–6** reveals that the vibrational sideband pattern of the photoluminescence spectra were observed for the complexes **1**, **2**, **3** and **6** whereas broad shape of the luminescence spectra were observed for complexes **4** and **5** as shown in Figs. 2a and b. Phosphorescent lifetime of the complexes **4** and **5** were obviously shorter than those of the complexes **1**, **2**, **3** and **6** and the radiative decay constant of complexes **1**, **2**, **3** and **6** are smaller than complexes **4** and **5** as shown in Table 1 and the same trend was observed by Okada et al. [38].

From the above results (the differences of vibrational structure, k_r, molar absorption co-efficient of singlet-triplet absorption peak and phosphorescent lifetime), the degree of mixing is taken into consideration to understand the photochemical differences of these complexes according to following Eq. (8)

$$\Phi_T = a\Phi_T(\pi - \pi^*) + b\Phi_T(MLCT) \quad (8)$$

Where, a and b are the normalized co-efficients and Φ_T (π-π^*) and Φ_T(MLCT) are the wave function of $^3\pi$-π^* and ^{3}MLCT excited states, respectively. For the iridium complex, the wave function of the triplet state (Φ_T) responsible for phosphorescence and Eq. 8 implies that the excited triplet state of the iridium complexes are mixture of Φ_T(π-π^*) and Φ_T(MLCT) [44, 45]. Therefore it can be concluded that the complexes **1**, **2**, **3** and **6** have excited state with large contribution of $^3\pi$-π^* whereas the complexes **4** and **5** have excited state with large contribution of ^{3}MLCT [38, 44, 46, 47].

Theoretical Approaches

The Mixing of Excited States

Calculations were performed using density functional theory (DFT) as implemented in the Gaussian-03 program [23]. The geometry optimization was carried out by B3LYP level using LANL2Z [24] basis set. The geometry optimization were carried out for $Ir(dmmppi)_2(acac)$ (**2**) and $Ir(dmdmppi)_2(acac)$ (**4**). The well known iridium complex $Ir(ppy)_3$ was used as a reference that had ^{3}MLCT dominant lowest excited state [38] for which the calculated Mulliken charge difference on iridium atom between the ground state and the lowest triplet excited state was 0.45. The calculation were done for **2** and **4** and the calculated Mulliken charges are 0.31 for $Ir(dmmppi)_2(acac)$ (**2**) and 0.43 for $Ir(dmdmppi)_2(acac)$ (**4**) and this result strongly supports that $^3\pi$-π^* is dominant for complex $Ir(dmmppi)_2(acac)$ (**2**) owing to small reduction of Mulliken charge on iridium when compared with $Ir(ppy)_3$ and ^{3}MLCT is dominant for complex $Ir(dmdmppi)_2(acac)$ (**4**) [23] owing to close to the value of $Ir(ppy)_3$.

HOMO-LUMO Orbitals of $Ir(dmmpfpi)_2(acac)$ (3)

The DFT calculations suggest that the highest occupied molecular orbital (HOMO) of these complexes are mainly localized on the phenyl rings of the phenylimidazole ligand

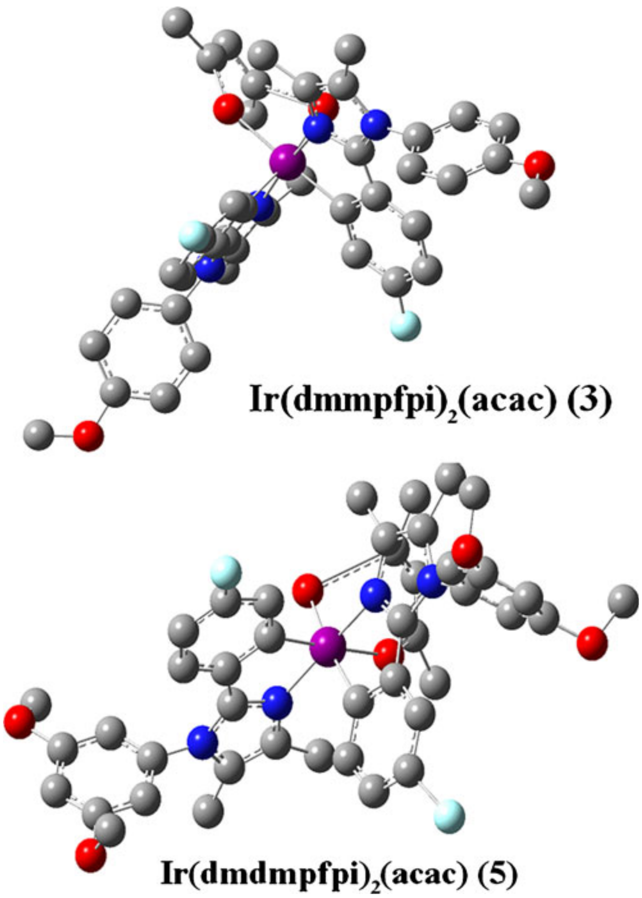

Fig. 10 The optimized structure of the complexes Ir(dmmpfpi)$_2$(acac) (**3**) Ir(dmdmpfpi)$_2$(acac) (**5**)

and iridium center. On the contrary, the lowest unoccupied molecular orbital (LUMO) is mainly localized on the phenyl ring attached to the carbon of the imidazole ring. The HOMO-LUMO orbital picture for the complex Ir (dmmpfpi)$_2$(acac) (**3**) is given in Fig. 8. The orbital picture predicts that variation is the electronic properties of the ligands should have an effect on the energy of the excited state and thereby confirmed the existence of remarkable photoinduced charge transfer properties [48].

Colour Tuning Based on DFT Calculations

On the basis of DFT calculation [23], the HOMO is localized the imidazole ring and iridium center and LUMO is localized on the phenyl ring attached to the carbon of the imidazole ring (Fig. 8). Therefore it is decided to substitute the electron withdrawing substituent (i.e., fluoro) at *para* position of the phenyl ring attached to the carbon of the imidazole ring and electron releasing substituent in the phenyl ring attached to the nitrogen of the imidazole ring for colour tuning (Fig. 9). From the emission peaks (Table 1) it was concluded that methoxy substituent on the benzaldeyde would cause a larger red shift in the emission spectra and it turns out that this expectation correlates well with the emission data [25].

Description of the Structure of Complexes Ir (dmmpfpi)$_2$(acac) 3 and Ir(dmdmpfpi)$_2$(acac) 5

From the optimized structures of iridium complexes, Ir (dmmpfpi)$_2$(acac) (**3**) and Ir(dmdmpfpi)$_2$(acac) (**5**) some selected bond lengths are presented in Table 4. From the Table 4 it was concluded that these complexes exhibit an octahedral geometry around iridium and prefers *cis*-C,C and *trans*-N,N chelate disposition instead of *trans*-C,C and *trans*-N,N chelate. Electron rich phenyl rings normally exhibit very strong influence and *trans* effect. Therefore, the *trans*-C,C arrangement is expected to be thermodynamically higher in energy and kinetically more labile [49]. This well known phenomenon referred to as transphobia [49, 50]. The Ir−C$_{av}$ bond of these complexes [Ir−C$_{av}$= 2.018 Å for Ir(dmmpfpi)$_2$(acac) (**3**) and 2.013 Å for Ir (dmdmpfpi)$_2$(acac) (**5**)] are found to be shorter than Ir−N$_{av}$ bond [Ir−N$_{av}$=2.049 Å for Ir(dmmpfpi)$_2$(acac) (**3**) and Ir(dmdmpfpi)$_2$(acac) (**5**)]. The Ir−C$_{av}$ bond length is similar to those in the analogues complexes reported [51, 52]. Furthermore the Ir−N$_{av}$ bond lengths also fall within the range of values for those of similar type of reported complexes [47, 50]. The Ir−O bond lengths [2.049 Å for Ir(dmmpfpi)$_2$(acac) (**3**) and 2.200 Å for Ir(dmdmpfpi)$_2$(acac) (**5**)] are longer than the mean Ir−O bond length (2.088 Å) reported and these observations reflect the *trans* influence of the phenyl groups. All other bond lengths and bond angles are analogous to the similar type of complexes [51, 52]. The optimized structure of complexes Ir(dmmpfpi)$_2$(acac) (**3**) and Ir(dmdmpfpi)$_2$(acac) (**5**) are shown in Fig. 10.

Conclusions

We have synthesized a series of Ir(III) complex dopants using various substituted imidazole ligands. These complexes exhibit different quantum efficiencies in solution depending upon the nature of substituents. The wavelength can be tuned by 63 nm depending upon the electronic properties of the substituents in the ligand. Some of the complexes discussed here showed ^{3}MLCT predominant mixing states for their lowest excited triplet states. But the degree of mixing between ^{3}MLCT and $^3\pi$-π* states of the excited states varied. From DFT calculation, the HOMO-LUMO orbital picture was determined and effort towards the development of RGB colour complexes using different substituents are currently underway and investigation of device studies for these iridium complexes are also currently in progress.

Acknowledgements One of the authors Dr. J. Jayabharathi, Reader in Chemistry, Annamalai University is thankful to Department of Science and Technology [No. SR/S1/IC-07/2007], University Grants Commission (F. No. 36-21/2008 (SR)) for providing fund to this research work and Prof. C. H. Cheng, Chairman, National Science Council, National Tsing Hua University for my post-doctoral research work.

References

1. Baldo MA, O'Brien DF, You Y, Shoustikov A, Thompson ME, Forrest SR (1988) Highly efficient phosphorescent emission from organic electroluminescent devices. Nature 395:151–154
2. Baldo MA, Thompson ME, Forrest SR (1999) Phosphorescent materials for application to organic light emitting devices. Pure Appl Chem 71:2095–2106
3. Gong X, Ostrowski JC, Bazan GC, Moses D, Heeger AJ (2002) Red electrophosphorescence from polymer doped with iridium complex. Appl Phys Lett 81:3711–3713
4. Adachi C, Baldo MA, Thompson ME, Forrest SR (2001) Nearly 100% internal phosphorescence efficiency in an organic light-emitting device. J Appl Phys 90:5048–5051
5. Ikai M, Tokito S, Sakamoto Y, Suzuki T, Taga Y (2001) Highly efficient phosphorescence from organic light-emitting devices with an exciton-block layer. Appl Phys Lett 79:156–158
6. Tokito S, Iijima T, Tsuzuki T, Sato F (2003) High-efficiency white phosphorescent organic light-emitting devices with greenish-blue and red-emitting layers. Appl Phys Lett 83:2459–2461
7. Lo S-C, Namdas EB, Burn PL, Samuel IDW (2003) Synthesis and properties of highly efficient electroluminescent green phosphorescent iridium cored dendrimers. Macromolecules 36:9721–9730
8. Kwong RC, Nugent MR, Michalski L, Ngo T, Rajan K, Tung Y-J, Weaver MS, Zhou TX, Hack M, Thompson ME, Forrest SR, Brown JJ (2002) High operational stability of electrophosphorescent devices. Appl Phys Lett 81:162–164
9. He G, Chang S-C, Chen F-C, Li Y, Yang Y (2002) Highly efficient polymer lightemitting devices using a phosphorescent sensitizer. Appl Phys Lett 81:1509–1512
10. Lee C-L, Lee KB, Kim J-J (2000) Polymer phosphorescent light-emitting devices doped with tris(2-phenylpyridine)iridium as a triplet emitter. Appl Phys Lett 77:2280–2282
11. Chen C-T (2004) Evolution of red organic light-emitting diodes: materials and devices. Chem Mater 16:4389–4400
12. Grushin VV, Herron N, LeCloux DD, Marshall WJ, Petrov VA, Wang Y (2001) New, efficient electroluminescent materials based on organometallic Ir complexes. Chem Commun 1494–1495
13. Bernhard S, Gao X, Malliaras GG, Abruna HD (2002) Efficient electroluminescent devices based on a chelated Osmium(II) complex. Adv Mater 14:433–435
14. Carlson B, Phelan GD, Kaminsky W, Dalton L, Jiang X, Liu S, Jen AKY (2002) Divalent osmium complexes: synthesis, characterization, strong red phosphorescence, and electrophosphorescence. J Am Chem Soc 124:14162–14172
15. Kim JH, Liu MS, Jen AKY, Carlson B, Dalton LR, Shu CF, Dodda R (2003) Bright red-emitting electrophosphorescent device using osmium complex as a triplet emitter. Appl Phys Lett 83:776–778
16. Tung YL, Wu PC, Liu CS, Chi Y, Yu JK, Hu YH, Chou PT, Peng SM, Lee GH, Tao Y, Carty AJ, Shu CF, Wu FI (2004) Highly efficient red phosphorescent osmium(II) complexes for OLED applications. Organometallics 23:3745–3748
17. Liu Z, Wang L, Chen J, Wang F, Ouyang X, Cao Y (2005) Synthesis and optoelectronic properties of silole-containing polyfluorenes with binary structures. J Polym Sci Pol Chem 45:756–767
18. Tung YL, Lee SW, Chi Y, Tao YT, Chien CH, Cheng YM, Chou PT, Peng SM, Liu CS (2005) Organic light-emitting diodes based on charge-neutral Os(II) emitters: generation of saturated red emission with very high external quantum efficiency. J Mater Chem 15:460–464
19. Kwong RC, Sibley S, Dubovoy T, Baldo M, Forrest SR, Thompson ME (1999) Efficient, saturated red organic light emitting devices based on phosphorescent platinum(II) porphyrins. Chem Mater 11:3709–3713
20. Che C-M, Hou Y-J, Chan MCW, Guo J, Liu Y, Wang Y (2003) [*meso*-Tetrakis-(pentafluorophenyl)porphyrinato]platinum(II) as an efficient, oxidation-resistant red phosphor: spectroscopic properties and applications in organic light-emitting diodes. J Mater Chem 13:1362–1366
21. Yoshinobu G, Noriko H, Motoyoshi Y (1970) Studies on azole compounds. II. Reaction of oxazole N-oxides with phenylisocyanate to give imidazole derivatives. Chem Pharm Bull 18:2000–2008
22. Nonoyama M (1974) Benzo(*h*)quinolin-10-yl-N iridium(III) complexes. Bull Chem Soc Jpn 47:767–768
23. Frisch MJ, Trucks GW, Schlegel HB, Scuseria GE, Robb MA, Cheeseman JR, Montgomery JA Jr., Vreven T, Kudin KN, Burant JC, Millam JM, Iyengar SS, Tomasi J, Barone V, Mennucci B, Cossi M, Scalmani G, Rega N, Petersson GA, Nakatsuji H, Hada M, Ehara M, Toyota K, Fukuda R, Hasegawa J, Ishida M, Nakajima T, Honda Y, Kitao O, Nakai H, Klene M, Li X, Knox JE, Hratchian HP, Cross JB, Adamo C, Jaramillo J, Gomperts R, Stratmann RE, Yazyev O, Austin AJ, Cammi R, Pomelli C, Ochterski JW, Ayala PY, Morokuma K, Voth GA, Salvador P, Dannenberg JJ, Zakrzewski VG, Dapprich S, Daniels AD, Strain MC, Farkas O, Malick DK, Rabuck AD, Raghavachari K, Foresman JB, Ortiz JV, Cui Q, Baboul AG, Clifford S, Cioslowski J, Stefanov BB, Liu G, Liashenko A, Piskorz P, Komaromi I, Martin RL, Fox DJ, Keith T, Al-Laham MA, Peng CY, Nanayakkara A, Challacombe M, Gill PMW, Johnson B, Chen W, Wong MW, Gonzalez C, Pople JA (2003) Gaussian, Inc., Pittsburgh
24. Minaev B, Mineva V, Agren H (2009) Theoretical study of the cyclometalated iridium(III) complexes used as chromophores for organic light emitting diodes. J Phys Chem A 113:726–735
25. Lamansky S, Djurovich P, Murphy D, Abdel-Razzaq F, Lee HE, Adachi C, Burrows PE, Forrest SR, Thompson ME (2001) Highly phosphorescent bis-cyclometalated iridium complexes: synthesis, photophysical characterization and use in organic light emitting diodes. J Am Chem Soc 123(4304):4312
26. Colombo MG, Guedel HU (1993) Synthesis and high-resolution optical spectroscopy of bis[2-(2-thienyl)pyridinato-C3, N](2, 2 -bipyridine)iridium(III). Inorg Chem 32:3081–3087
27. Demas JN, Taylor DG (1979) On the "intersystem crossing" yields in ruthenium(II) and osmium(II) photosensitizers. Inorg Chem 18:3177–3179
28. Damrauer NH, Boussie TR, Devenney M, McCusker JK (1997) Effect of intraligand electron delocalization, steric tuning, and excited-state vibronic coupling on the photophysics of aryl-substituted bipyridyl complexes of Ru(II). J Am Chem Soc 119:8253–8268
29. Djurovich P, Murphy D, Abdel-Razzag F, Kwong R, Tsyba I, Bortz M, Mui B, Bau R, Thompson ME (2001) Synthesis and characterization of phosphorescent cyclometalated iridium complexes. Inorg Chem 40:1704–1711
30. Colombo MG, Gwelel HU (1993) Synthesis and high-resolution optical spectroscopy of bis[2-(2-thienyl)pyridinato-C3, N′](2, 2′-bipyridine)iridium (III). Inorg Chem 32:3081–3087
31. Tang K-C, Liu KL, Chen IC (2004) Rapid intersystem crossing in highly phosphorescent iridium complexes. Chem Phys Lett 386:437–441

32. Mi B-X, Wang PF, Liu M-W, Kwong H-L, Wong N-B, Lee CS, Lee ST (2003) Thermally stable hole-transporting material for organic light emitting diode: an isoindole derivative. Chem Mater 15:3148–3151
33. Gange RR, Koval CA, Lisensky GC (1980) Ferrocene as an internal standard for electrochemical measurements. Inorg Chem 19:2854–2855
34. Ranjan S, Lin SY, Hwang KC, Chi Y, Ching WL, Liu CS, Tao YT, Chien CH, Peng SM, Lee GH (2003) Realizing green phosphorescent light-emitting materials from rhenium(I) complexes. Inorg Chem 42:1248–1255
35. Hay PJ (2002) Theoretical studies of the ground and excited electronic states in cyclometalated phenylpyridine Ir(III) complexes using density functional theory. J Phys Chem A 106:1634–1641
36. Sudhakar M, Djurovich PI, Hogen-Esch TE, Thompson ME (2003) Phosphorescence quenching by conjugated polymers. J Am Chem Soc 125:7796–7797
37. Chen FC, He G, Yang Y (2003) Triplet exciton confinement in phosphorescent polymer light-emitting diodes. Appl Phys Lett 82:1006–1008
38. Okada S, Okinaka K, Iwawaki H, Furugori M, Hashimoto M, Mukaide T, Kamatani J, Igawa S, Tsuboyama A, Takiguchi T, Ueno K (2005) Substituent effect of iridium complexes for highly efficient red OLEDs. Dalton Trans 15:83–1590
39. Chen H-Y, Chi Y, Liu C-S, Yu J-K, Cheng Y-M, Chen K-S, Chou P-T, Peng S-M, Lee G-H, Carty AJ, Yeh S-J, Chen C-T (2005) Rational colour tuning and luminescent properties of functionalized boron-containing 2-pyridyl pyrrolide complexes. Adv Funct Mater 15:567–574
40. King KA, Spellane DJ, Watts RJ (1985) Excited-state properties of a triply *ortho*-metalated iridium(III) complex. J Am Chem Soc 107:1431–1432
41. Baldo MA, Lamansky S, Burrows PE, Thompson ME, Forrest SR (1999) Very high-efficiency green organic light-emitting devices based on electrophosphorescence. Appl Phys Lett 75:4–6
42. Brooks J, Babayan Y, Lamansky S, Djurovich PI, Tsybu I, Bau R, Thompson ME (2002) Synthesis and characterization of phosphorescent cyclometalated platinum complexes. Inorg Chem 41:3055–3066
43. Cummings SD, Eisenberg R (1996) Tuning the excited-state properties of platinum(II) diimine dithiolate complexes. J Am Chem Soc 118:1949–1960
44. Tamayo AB, Alleyne BD, Djurovich PI, Lamansky S, Tsyba I, Ho NN, Bau R, Thompson ME (2003) Synthesis and characterization facial and meridional tris-cyclometalated iridium(III) complexes. J Am Chem Soc 125:7377–7387
45. Tsuboyama A, Iwawaki H, Frugori M, Mukaide T, Kamatain J, Igawa S, Moriyama T, Miura S, Takiguchi T, Okada S, Hoshino M, Ueno K (2003) Homoleptic cyclometalated iridium complexes with highly efficient red phosphorescence and application to organic light-emitting diode. J Am Chem Soc 125:12971–12979
46. Colombo MG, Hauser A, Guedel HU (1993) Evidence for strong mixing between the LC and MLCT excited states in bis(2-phenylpyridinato-C2, N′)(2, 2′-bipyridine)iridium(III). Inorg Chem 32:3088–3092
47. Okada S, Iwawaki H, Frugori M, Mukaide J, Kermatami J, Igawa S, Moriyama T, Miuva S, Tsuboyama A, Takiguchi T, Mizutami H (2002) In: Morreale J (ed) Society for information on display, SID Symp. Drig., Scan Jose CA, USA (2002) 1360
48. Cheng C-C, Yu W-S, Chou P-T, Peng S-M, Lee G-H, Wu P-C, Song Y-H, Chi Y (2003) Syntheses and remarkable photophysical properties of 5-(2-pyridyl)pyrazolate boron complexes: photoinduced electron transfer. Chem Commun 628–2629
49. Vicente J, Arcas A, Bautista D, de Arellano MCR (2002) Mono- and di-nuclear complexes of ortho-palladated and -platinated 4, 4′-dimethylazobenzene with bis(diphenylphosphino)methane. More data on transphobia. J Organomet Chem 663:164–172
50. Hwang GT, Son HS, Ku JK, Kim BH (2003) Synthesis and photophysical studies of bis-enediynes as tunable fluorophores. J Am Chem Soc 125:11241–11248
51. Urban R, Kramer R, Mihan S, Polborn K, Wagner B, Beck W (1996) Metal complexes of biologically important ligands, LXXXVII -amino carboxylate complexes of palladium(II), iridium(III) and ruthenium(II) from chloro-bridged orthometalated metal compounds and [(OC)3Ru (Cl)(-Cl)]2. J Organomet Chem 517:191–200
52. Neve F, Crispini A (2000) Metal-containing amphiphiles: ortho-metalated iridium(III) complexes with substituted 6 -phenyl-2,2 -bipyridines. Eur J Inorg Chem 1039–1043